ACS OMEGA

http://pubs.acs.org/journal/acsodf

Article

Hierarchically Porous, Biphasic, and C-Doped TiO_2 for Solar Photocatalytic Degradation of Dyes and Selective Oxidation of Benzyl Alcohol

R. Ragesh Nath, C. Nethravathi,* and Michael Rajamathi

Cite This: *ACS Omega* 2021, 6, 12124−12132

Read Online

ACCESS | Metrics & More | Article Recommendations | Supporting Information

ABSTRACT: Macroporous TiO_2 monoliths were synthesized by self-sustained combustion reactions of molded pellets made up of a mixture of $TiCl_4$ as a precursor, urea as a fuel, ammonium nitrate as an oxidizer, and starch as a binder. The porous TiO_2 monoliths were found to be a heterostructure of anatase and rutile phases, in addition to being doped with carbon. Variation in the amount of starch yielded porous monoliths of different anatase−rutile ratios (increasing rutile component from 0 to 40%) but comparable Brunauer−Emmett−Teller (BET) surface area (~30 m^2 g^{-1}). The porous monoliths obtained, where the $TiCl_4$/starch mass ratio was 2.17, exhibit exceptional photocatalytic activity in the degradation of dyes (methylene blue and methyl orange) and selective oxidation of benzyl alcohol to benzaldehyde under natural sunlight. The synergistic combination of high surface area, porous network, lowered band gap due to heterostructured anatase−rutile polymorphs, and the presence of doped carbon renders the macroporous TiO_2 an efficient photocatalyst.

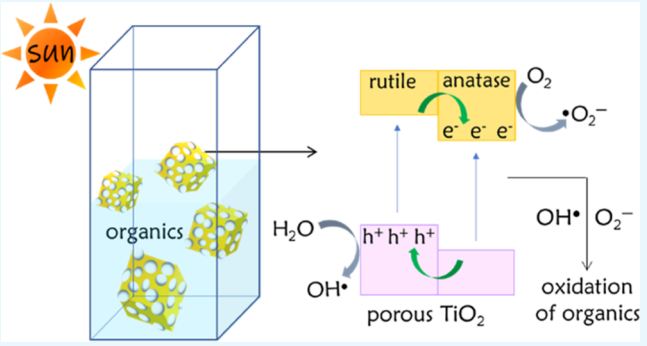

1. INTRODUCTION

TiO_2 photocatalysts[1] have been of interest, as they facilitate the photocatalytic degradation of organic pollutants,[2−6] selective organic transformations,[7−11] and hydrogen generation by photocatalytic water splitting.[12−14] Adsorbed radicals formed by photogenerated electron−hole pairs at the photocatalyst surface cause photocatalytic reactions.[15,16] TiO_2 exists in three polymorphic forms—anatase, rutile, and brookite.[1,15,16] The anatase phase has been found to exhibit higher photocatalytic efficiency.[17,18] While anatase with a band gap of 3.2 eV is confined to absorption of UV light, rutile with a lower band gap (3.0 eV) can absorb visible light. However, low surface area, low redox potential, and faster electron−hole recombination render rutile ineffective.[19] There has been immense interest to modify TiO_2 to enable it to absorb a wide range of wavelengths of solar energy,[1,15,16] including the visible region.[2,7,15,16,19] This has been achieved through various methods—metal[20,21] or nonmetal doping,[21,22] creating oxygen deficiency to form TiO_{2-x},[23] dye sensitization[15,16] or making TiO_2−quantum dots heterostructures.[15,16,24] Factors such as the concentration and nature of the dopant, crystallite size, surface area, and anatase−rutile ratio[2,4−6,14,19] control the photocatalytic efficiency of TiO_2.

Commercially available TiO_2 (Degussa P25) is a biphasic interfacial heterojunction of anatase−rutile (80:20).[6,19,25] Bickley et al.[25] were the first to propose a synergetic effect between anatase and rutile to be responsible for the relatively high photoreactivity of Degussa P25, in comparison to pure anatase or rutile.[25] This is because the close proximity of anatase and rutile polymorphs results in two key processes:[6,19,25−28] (1) the rutile phase with a lower band gap not only facilitates the production of charges in the visible light region but also transfers these charges to the conduction band of the anatase phase and eventually to the surface sites and (2) photogenerated holes from the valence band of anatase can be effectively transferred to that of rutile, thus leading to slow electron−hole recombination.[6,26] It would be ideal to improve the efficiency of materials similar to Degussa P25.[6,19] Major concerns in the preparation of compositions similar to Degussa are: (1) anatase−rutile mixtures are generally formed above 600 °C, yielding TiO_2 samples that deviate from nanoregime, and hence reduce the surface area, leading to a decrease in photocatalytic efficiency[29] and (2) nitrogen doping stabilizes the anatase phase at higher temperatures, thus preventing the formation of a biphasic mixture.[30]

Anatase−rutile mixtures of TiO_2 have been synthesized by calcination of the products obtained by solvothermal[5,17] and sol−gel[6,19] methods or through direct combustion.[29] Rutile−

Received: February 15, 2021
Accepted: April 19, 2021
Published: April 28, 2021

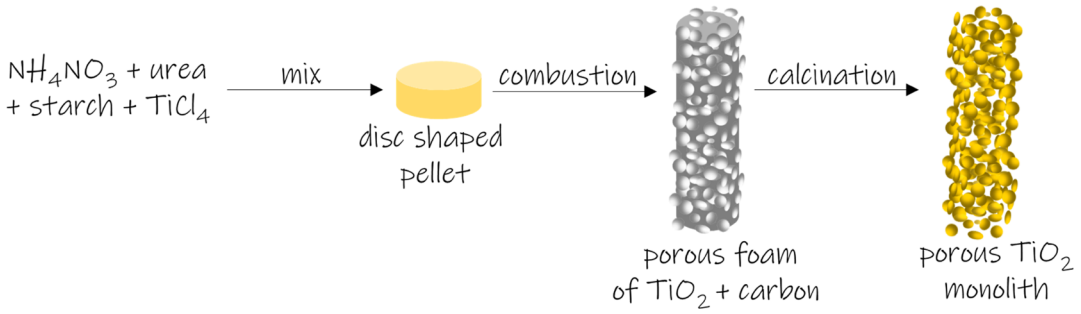

Figure 1. Schematic of the processes involved in the formation of porous C-doped TiO_2.

anatase branched heterostructures were prepared by a combination of electrospinning and the hydrothermal reaction.[31] Patterned anatase−rutile junctions have been formed by calcination of patterned TiO_2 gel films.[32] Pulsed-pressure MOCVD has been used to fabricate anatase−rutile heterojunctions.[14] Porous films of TiO_2 mixtures have been prepared through plasma electrolytic oxidation (PEO).[33] Heterogeneous nanostructures of anatase nanoparticles on rutile nanorods were synthesized through layer-by-layer, electrostatic deposition.[34] Though the existing synthesis routes yield anatase−rutile mixtures/heterojunctions, in most cases, multistep reactions are involved and only a few of them yield porous products. While it is important to find simpler scalable methods for anatase−rutile mixtures of suitable ratios, it would also be of interest to obtain these in the form of light-weight porous monoliths so that these could be used as floats[35] in water bodies for pollutant degradation applications. Our group has developed a self-sustained combustion synthesis of metal oxide foams using starch-based molded pellets.[36,37] For example, t-ZrO_2 monolithic foams could be obtained by subjecting a pellet made up of $ZrO(NO_3)_2$, urea, and starch.[37] Adapting this method,[36,37] in this work, we have synthesized macroporous monoliths of anatase−rutile TiO_2. The excess of carbon in the reaction mixture ensured carbon doping (C-doping) of TiO_2. These monoliths are found to be quite efficient in natural sunlight photocatalysis.

2. EXPERIMENTAL SECTION

2.1. Synthesis of Porous TiO_2 by the Combustion Method. Macroporous TiO_2 was prepared by the combustion method using $TiCl_4$ as a precursor, urea as a fuel, ammonium nitrate as an oxidizer and starch as a binder. Urea (0.011 mol, 0.7125 g) was mixed with 0.8435 g of ammonium nitrate (0.01 mol), starch, and 0.5 mL of $TiCl_4$ (0.86 g, 0.004 mol). The resulting mixture was ground into a dough-like consistency that could be molded into pellets of the desired shape. The mass of starch was varied from 100 to 2000 mg. The pellet was placed in a preheated crucible (800 °C) in an electric Bunsen. Instantly, a vigorous reaction was observed with the formation of an oxide foam. The oxide foam was heated in air at 800 °C for 20 min to burn away the organic remnants.

2.2. Photocatalytic Degradation of Dyes. Macroporous TiO_2 (10 mg) was dispersed in 100 mL of the dye solution (10 mg L^{-1}). The solution was stirred in the dark for 1 h. After attaining the equilibrium, the solution was irradiated with natural sunlight. Aliquots were collected periodically, and the catalyst was removed by centrifugation. The dye concentration was monitored by measuring the absorbance of methylene blue (MB) at 664 nm and that of methyl orange (MO) at 464 nm.

2.3. Photocatalytic Selective Oxidation of Alcohol. Macroporous TiO_2 (10 mg) and 10 μL of benzyl alcohol (0.1 mmol) were added to 1.5 mL of oxygen saturated benzotrifluoride (BTF). The solution was stirred in the dark for 0.5 h. The solution was then transferred into a Pyrex glass filled with oxygen. The solution was irradiated with direct sunlight. After the reaction, the catalyst was removed by centrifugation. High-performance liquid chromatography (HPLC) was used to monitor the oxidation of the alcohol.

2.4. Characterization. The samples were characterized by X-ray diffraction (XRD) using a PANalytical X'pert pro diffractometer (Cu Kα radiation, secondary graphite monochromator, scanning rate of 1° 2θ/min). IR spectroscopic studies were carried out in a PerkinElmer FTIR spectrophotometer (spectrum two) in the range from 4000 to 550 cm^{-1} with a resolution of 4 cm^{-1}. X-ray photoelectron spectra (XPS) of the samples were recorded using a Kratos axis Ultra DLD. Scanning electron microscopy (SEM) images were recorded using a Zeiss, Ultra 55 field emission scanning electron microscope. A PerkinElmer LS 35 spectrometer was used to record the UV−visible spectra. The catalytic oxidation of benzyl alcohol was monitored by HPLC (Jasco) using a C18 column and a UV detector at 253 nm. A mixture of water and acetonitrile in a 70:30 volume ratio and 0.2 M phosphoric acid was used as the mobile phase. The mobile phase flow rate was maintained at 0.8 mL min^{-1}. The nitrogen sorption analysis was performed in a BELsorp mini-II instrument at liquid nitrogen temperature. The surface area of the material was determined by employing the Brunauer−Emmett−Teller equation. The pore sizes and pore volumes of the materials were obtained by the Barrett−Joyner−Halenda (BJH) method.

3. RESULTS AND DISCUSSION

The processes involved in the formation of porous TiO_2 monoliths by the starch pellet combustion method are schematically depicted in Figure 1. Once the combustion is initiated, the pellet catches fire and grows into a voluminous cylindrical foamy product, with its radius comparable to the radius of the initial pellet, within a few seconds. Partial burning of starch leaves behind a lot of carbonaceous impurities at this stage. Further heating in air burns away these impurities leaving behind a porous monolith of TiO_2.

3.1. Catalyst Characterization. The XRD patterns of macroporous TiO_2 obtained by combustion synthesis with varying amounts of starch are shown in Figure 2. All of the peaks could be assigned to the anatase phase in the case of TiO_2 prepared in the presence of 100 mg of starch (Figure 2a). Peaks due to the rutile phase of TiO_2 are observed on increasing the mass of starch to 250 mg and above (Figure 2b−g). With an

https://doi.org/10.1021/acsomega.1c00825
ACS Omega 2021, 6, 12124−12132

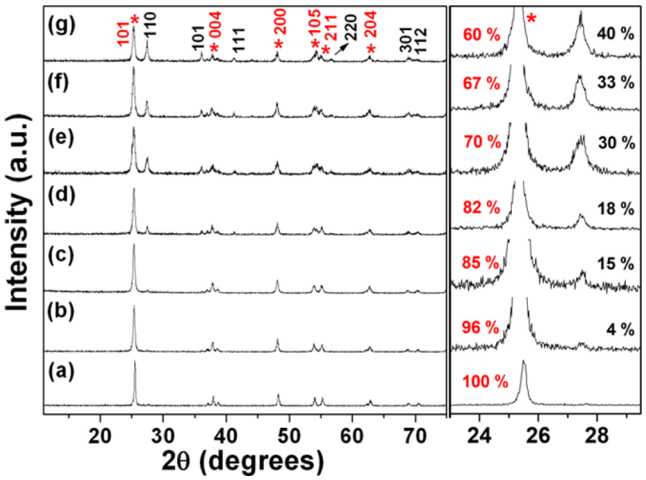

Figure 2. XRD patterns of porous TiO_2 synthesized using (a) 100, (b) 250, (c) 350, (d) 500, (e) 750, (f) 1000, and (g) 2000 mg of starch. Peaks indicated as (*) are due to the anatase phase coexisting with the rutile phase. The expanded region (20−30°) is shown in the right hand side panel. The percentages of the anatase and rutile phases were obtained from the relative intensities of the 101 reflection of anatase and 110 reflection of rutile, respectively.

increase in the mass of starch used in the synthesis (100−2000 mg), the percentage of the rutile phase also increases (0−40%) gradually. Though the reaction has been carried out at 800 °C (the actual local temperature in the reaction mixture would be even higher due to the exothermic combustion reaction), the stable anatase phase is observed in contrast to studies that indicate stabilization of the rutile phase at temperatures above 600 °C. Even with 2 g of starch ($TiCl_4$/starch ratio of 0.38), the anatase phase is largely stabilized with only 40% of the rutile phase being present in the product. (Figure 2, right hand side panel).

The Spurr equation $F_R = 1/\{1+0.8[I_A(101)/I_R(110)]\}$ was employed for the precise calculation of the amount of rutile in the sample,[19] where F_R is the mass fraction of rutile and I_A (101) and I_R (110) are the integrated main peak intensities of anatase and rutile, respectively. The rutile content increases with an increase in the amount of starch used (Figure S1, Supporting Information), suggesting that an increase in starch content leads to the destabilization of the anatase phase. Thus, the starch-based combustion method allows one to easily synthesize an array of TiO_2 materials with different anatase−rutile ratios.

The chemical composition of TiO_2 was further probed using X-ray photoelectron spectroscopy (XPS). The Ti 2p spectrum (Figure 3a) shows peaks (458.77 and 464. 47eV) due to Ti^{4+}. The core-level C 1s spectrum (Figure 3b) exhibits peaks at 284.95, 286.47, and 288.86 eV that are ascribed to adventitious carbon from the internal standard, −C−O, and −C═O, respectively. No peaks due to Ti−C (281 eV) were observed, indicating that carbon is not in the substitutional lattice position.[29,38] These features suggest that carbon could be in the interstitial position of the TiO_2 lattice or as carbonate species at the surface.[39,40] The infrared spectrum (Figure S2, Supporting Information) further corroborates the existence of −C−O species along with strong −O−H stretching and bending absorptions, indicating the interaction of moisture with surface carboxylate species.[29,38,39,41] The N 1s spectrum (not shown) indicates the absence of nitrogen in the sample. These observations are in accordance with the literature for C-doped TiO_2.[29,38,39]

The UV−visible absorbance spectrum (Figure 3c) of porous TiO_2 (350 mg of starch) exhibits a broad absorption range in the visible region with a band gap of 2.51 eV calculated from the Tauc plot (the inset of Figure 3c). In comparison to theoretical 3.00 and 3.20 eV for rutile and anatase, respectively, narrowing of the band gap in porous TiO_2 is due to anatase−rutile heterojunctions in addition to contributions of dopants and defects as indicated by XPS studies.[19,38]

The SEM images (Figure 4a,b) of TiO_2 (350 mg of starch) show an irregularly shaped, coral-like, highly porous network with macropores of diameters of ∼1 μm. The porous nature is further corroborated by the BET surface area measurements (Figure 4e,f). The surface area is measured to be 33.4 $m^2\ g^{-1}$ with a pore volume of 0.12 $cm^3\ g^{-1}$ and a mean pore diameter of 14.6 nm, suggesting that TiO_2 obtained using 350 mg of starch exhibits macro- and mesopores. In comparison, the SEM image of TiO_2 (2000 mg of starch) comprises sheets (Figure 4c,d) that are in μm size laterally without any visible macropores. The surface area is measured to be 28.5 $m^2\ g^{-1}$, with a pore volume of 0.009 $cm^3\ g^{-1}$ and a mean pore diameter of 14.0 nm, indicating that the material is mesoporous.

3.2. Mechanism of Formation of Anatase−Rutile Biphasic Porous TiO_2. The anatase−rutile transformation is reconstructive, wherein the transformation involves the breaking and reforming of bonds.[42] As suggested in the previous studies,[36,37] the amount of starch and $\Delta G°(f)$ of the metal oxide are expected to control the porosity of the material. The

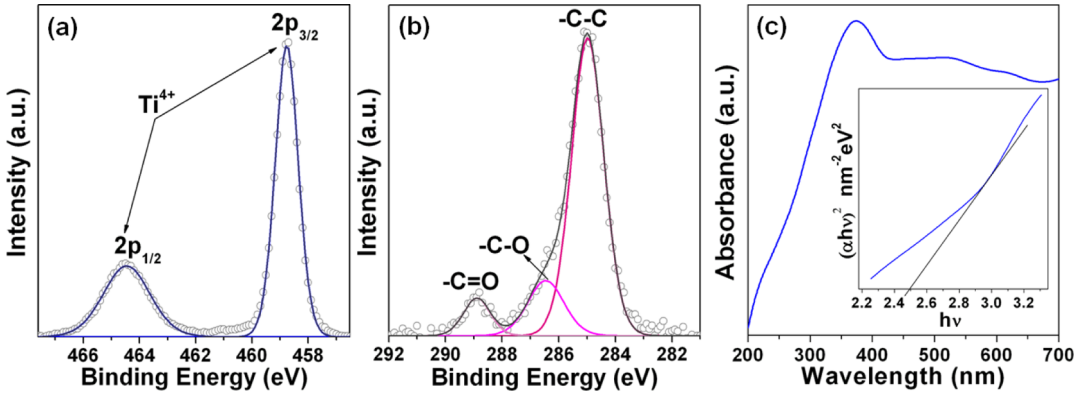

Figure 3. XPS spectra showing (a) Ti 2p and (b) C 1s core-level peak regions. (c) UV−visible reflectance spectrum of porous TiO_2 (synthesized using 350 mg of starch).

https://doi.org/10.1021/acsomega.1c00825
ACS Omega 2021, 6, 12124−12132

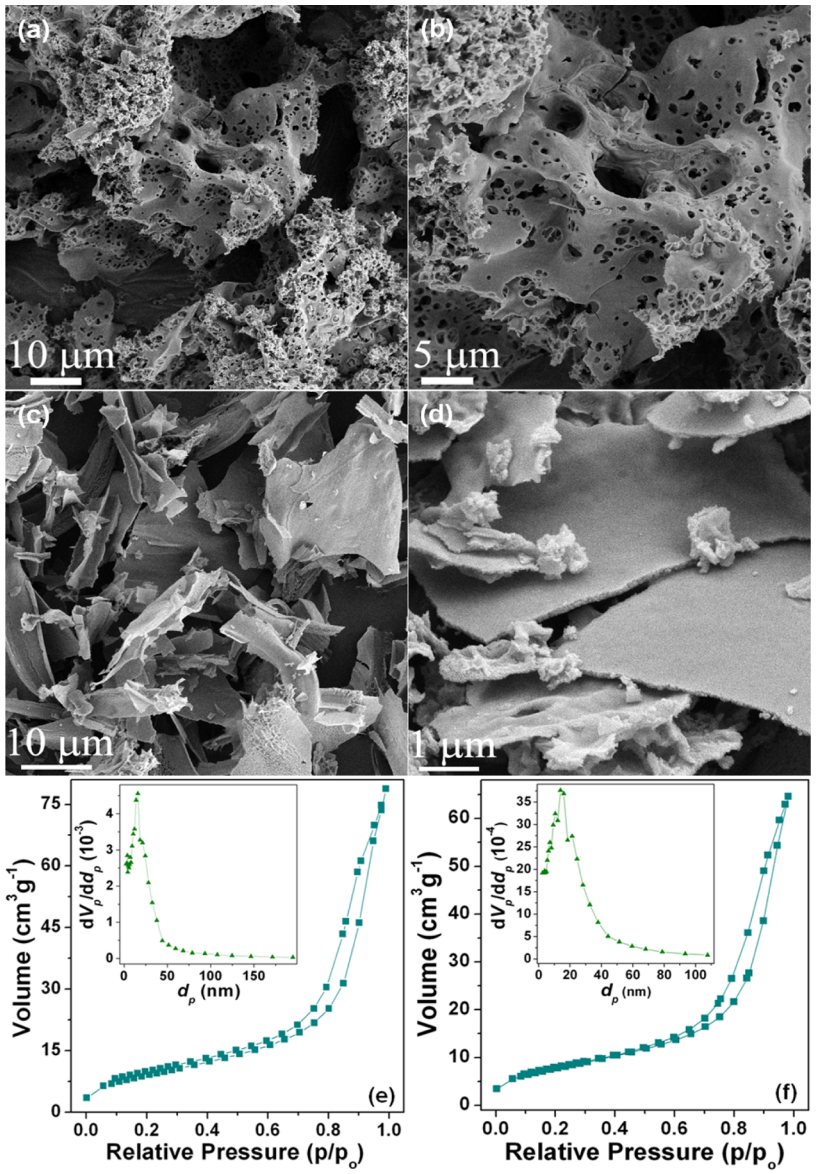

Figure 4. Bright-field SEM images of porous TiO_2 prepared using 350 mg of starch (a, b) and 2000 mg of starch (c, d). Nitrogen adsorption−desorption isotherms of porous TiO_2 prepared using 350 mg of starch (e) and 2000 mg of starch (f). The insets in (e, f) are the corresponding BJH plots.

amount of gases evolved depends on the mass of starch used. The energy released (ΔG°) during the reaction decides the local temperature. All of the reactions, using different amounts of starch, have been carried out under similar heating conditions. During combustion, the internal temperature is expected to increase when a higher mass of starch is being burnt, thus resulting in anatase−rutile transformation. However, experimental observations suggest that the internal temperature decreases with increasing amounts of starch.[37] With a higher amount of starch, burning of starch through self-sustained combustion is slow, resulting in the lowering of the overall temperature. The reason for lower rutile content in the products seems to be purely kinetic. The total reaction time is ∼20 min, which is insufficient to convert the initially formed anatase into rutile. The increased rutile content with an increase in starch may be attributed to the reductive atmosphere created by starch. During combustion, starch is dehydrated to give carbon, which being reductive in nature results in oxygen vacancies, leading to an increased rate of transformation of anatase to rutile.[42]

As the $\Delta G^\circ(f)$ of TiO_2 is the same for reactions using 350 and 2000 mg of starch, the surface area and porosity solely depend on the nature of combustion of starch. With lower amounts of starch, the temperature is sufficient to cause high rates of the reaction, resulting in the local pressure build up and coral-like combusted products. As the starch content increases, the reaction proceeds at a lower rate, analogous to the smoldering of a cigarette stick.[37] This is conducive to the formation of anisotropic products, as starch−sponge template could burn rapidly, uniformly leading to interconnected thin, porous sheets.

3.3. Photocatalytic Performance of Anatase−Rutile Biphasic Porous TiO_2 in Dye Degradation. The photocatalytic efficiency of porous TiO_2 prepared with varying amounts of starch was examined by monitoring the degradation of methylene blue under solar irradiation. The photocatalytic activity of porous TiO_2 summarized in Table 1 suggests that

https://doi.org/10.1021/acsomega.1c00825
ACS Omega 2021, 6, 12124−12132

Table 1. Summary of the Solar Photocatalytic Degradation of Methylene Blue (100 mL, 10 ppm) using 10 mg of Porous TiO_2 Synthesized using Varying Amounts of Starch

	% composition		MB degradation		
starch (mg)	anatase	rutile	adsorption (%)	degradation (%)	time (min)
100	100	0	0	0	120
250	96	4	4	80	120
350	85	15	6	100	80
500	82	18	12	100	110
750	70	30	19	100	120
1000	67	33	30	100	120
2000	60	40	42	100	120

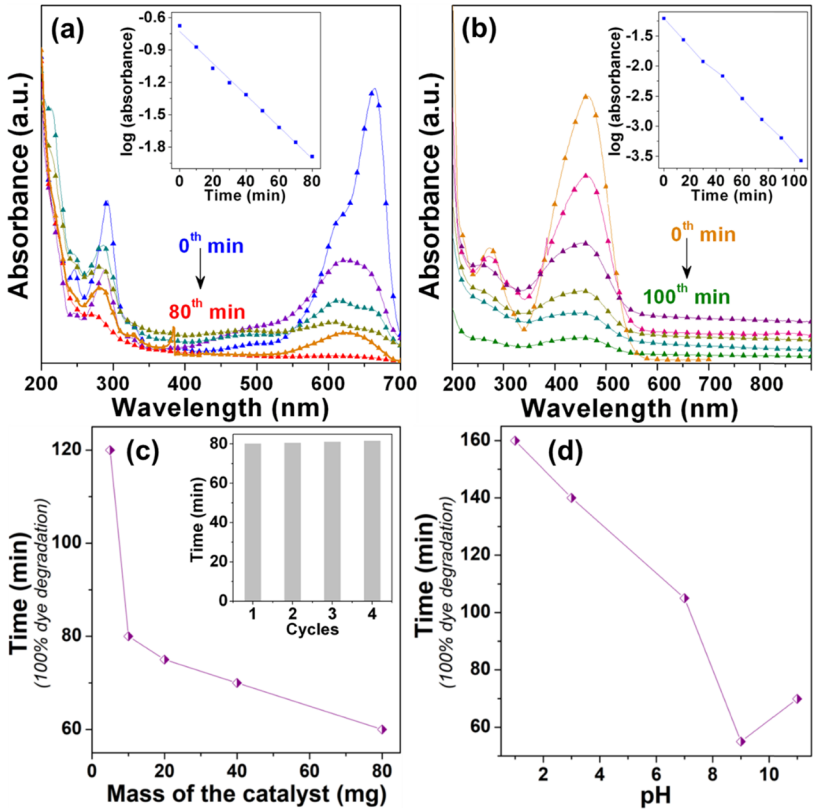

Figure 5. Degradation of dyes (10 mg L^{-1}) was traced through UV−visible absorption spectra of reaction mixtures containing 10 mg of porous TiO_2 heterojunctions as a photocatalyst. Evolution of absorption spectra with time in the case of (a) MB and (b) MO, and the insets correspond to log (absorbance) versus time plots. Variation of the photocatalytic MB (100 mL, 10 mg L^{-1}) degradation efficiency with (c) mass of porous TiO_2 heterojunctions as a catalyst and (d) pH. Catalytic efficiency over repeated cycles in the case of MB degradation is shown as the inset in (c).

TiO_2 prepared with lower starch content degrade the dye with minimum adsorption in comparison to TiO_2 prepared using a higher amount of starch. The UV−visible spectra of the dye extracted from the catalytic sample indicate that the reaction in the dark is adsorption and not degradation. The increased adsorption with the use of increased amounts of starch could be attributed to the increased surface −O−H and −C−O as the starch content increases, though the surface areas of all of the samples are comparable.

The photocatalytic activity of porous TiO_2 (350 mg of starch) in the degradation of MB and MO was evaluated under direct solar light. In all of the cases, prior to photocatalytic degradation, adsorption−desorption equilibrium in the dark indicates negligible or low adsorption. Figure 5a,b represents the time-resolved UV−visible absorption spectra of photocatalytic degradation of MB and MO, respectively. In both cases, the intensity of the prominent absorption decreases with time. The log (absorbance) versus time plots (insets of Figure 5a,b) of MB and MO degradation indicate pseudo-first-order kinetics with rate constants of 0.034 and 0.0511 min^{-1}, respectively. Over four degradation cycles (the inset of Figure 5c), porous TiO_2 (prepared with 350 mg of starch) exhibits consistent catalytic activity. Adsorbed water and oxygen on the surface of TiO_2 produce reactive $^{\bullet}OH$ and $^{\bullet}O^{2-}$ in the presence of sunlight. Degradation takes place only in the presence of a catalyst and sunlight (Table S1, Supporting Information) due to the increased concentration of net oxidizing species in solution. Nonlinear dependency on the amount of the catalyst appears to be exponential with saturation beginning at 10 mg of the catalyst (Figure 5c).

One of the requisites of an ideal catalyst is its ability to catalyze the degradation of organics under all pH conditions. The effect of pH on the degradation of MB (Figure 5d) clearly indicates that porous TiO_2 effectively catalysize dye degradation in a wide

https://doi.org/10.1021/acsomega.1c00825
ACS Omega 2021, 6, 12124−12132

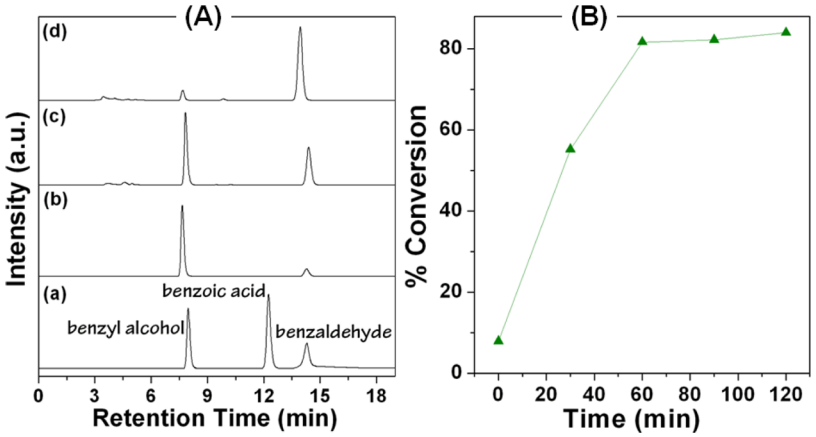

Figure 6. (A) HPLC chromatograms of (a) standard equimolar solution of benzyl alcohol, benzoic acid, and benzaldehyde, and solutions obtained by photooxidation of benzyl alcohol catalyzed by porous TiO_2 (prepared using 350 mg of starch) in the presence of oxygen saturated benzotriflouride (BTF) at (b) 1st, (c) 30th, and (d) 60th min, respectively. (B) Plot of the percentage conversion of benzyl alcohol with respect to time.

pH range (1−11) and more efficiently in basic pH due to the higher concentration of intermediate radicals.[6,41]

3.4. Photocatalytic Performance of Anatase−Rutile Biphasic Porous TiO_2 in Selective Oxidation of Benzyl Alcohol. The photocatalytic oxidation of many organic molecules by optically excited TiO_2 is thermodynamically feasible at room temperature in the presence of oxygen.[11] The photogenerated holes with an oxidation potential of 3.0 V renders TiO_2 with considerable oxidizing capability.[11,43] Benzaldehyde is a widely used raw material in pharmaceutical industries. Benzaldehyde is synthesized through selective oxidation of benzyl alcohol using liquid-phase chlorination, a toxic and corrosive process.[11,44] It is of importance to develop alternative chlorine-free routes to produce benzaldehyde.[44,45] In the presence of noble metal[46] or transition metal complexes[47] as catalysts, molecular oxygen has emerged as a primary oxidant in the oxidation of alcohols to carbonyl compounds.[11,44−46] Photocatalytic selective organic transformations,[44−47] utilizing renewable solar energy, have garnered interest as a greener and efficient route.[44−46] Environmentally benign, economically viable, and naturally abundant TiO_2 has been explored as a potential photocatalyst in selective oxidation of benzyl alcohol.[11,43−47]

Benzyl alcohol interacts with the surface hydroxyl groups of the photoexcited porous TiO_2. The photogenerated holes in TiO_2 abstract the protons from benzyl alcohol, while the alcohol loses an electron and gets oxidized to aldehyde. The longer surface adsorption of the reactant (alcohol) or the product (aldehyde) not only leads to a decrease in the photocatalytic activity of TiO_2 but also leads to further oxidation of aldehyde to acid, thus minimizing the selectivity of the oxidation process.

The porous TiO_2 (prepared using 350 mg of starch) heterostructure exhibits excellent photocatalytic activity toward selective oxidation of benzyl alcohol to benzaldehyde. The HPLC chromatograms of the aliquots of the reaction mixture taken at different time intervals (Figure 6A) show a gradual decrease in the concentration of alcohol and a corresponding increase in the concentration of aldehyde with the concentration of the acid being zero at all times, indicating 100% selectivity. A conversion of 80% with 100% selectivity was achieved in 60 min (Figure 6B). The conversion and selectivity are defined as follows

$$\text{conversion percentage} = (C_o - C_{alcohol})/C_o \times 100$$

$$\text{selectivity percentage} = C_{aldehyde}/(C_o - C_{alcohol}) \times 100$$

C_o is the initial concentration of benzyl alcohol, $C_{alcohol}$ and $C_{aldehyde}$ are the concentrations of benzyl alcohol and benzyaldehyde, respectively, at a given reaction time. However, beyond 60 min, the progress of the reaction was quite slow and a conversion percentage of 87 was observed after 120 min. The catalyst could be recovered and reused to get similar results over four cycles.

3.5. Reasons for the Enhanced Photocatalytic Performance of Anatase−Rutile Biphasic Porous TiO_2. Adsorbed water and oxygen on the surface of porous TiO_2 monoliths produce reactive $^{\bullet}OH$ and $^{\bullet}O^{2-}$ in the presence of sunlight. These radicals cause degradation of the dye. The porous monolith architecture of TiO_2 facilitates the formation of more heterojunctions, thereby increasing the activity. With the conduction band edge of rutile ∼0.2 eV lower than that of anatase, the photoexcited electrons are effectively transferred from the conduction band of rutile to that of anatase at the interface between anatase and rutile.[6,26] While this promotes photoreduction at the anatase site (Figure 7), photooxidation takes place either on the anatase or rutile surface.

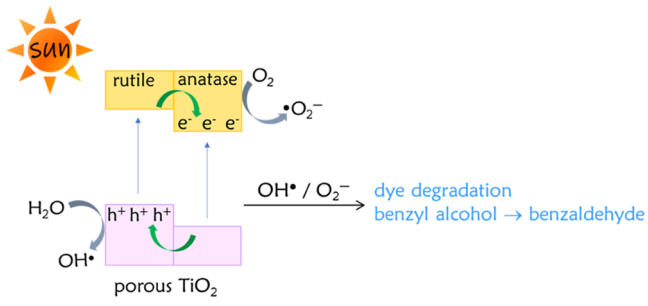

Figure 7. Schematic of the processes involved in the sunlight photocatalytic activity of porous biphasic C-doped TiO_2 monoliths.

The photocatalytic performance of all of the porous TiO_2 monoliths is higher than that of commercial Degussa P25. This is attributed to the following reasons: (1) a porous network provides channels for faster reactant diffusion and more active catalytic sites, (2) anatase−rutile heterojunctions aid in electron−hole separation and a wider range of solar energy absorption, and (3) doped carbon not only contributes to the

https://doi.org/10.1021/acsomega.1c00825
ACS Omega 2021, 6, 12124−12132

Table 2. Comparison of Photocatalytic Activities of Porous TiO_2 (350 mg of Starch) with other TiO_2 Catalysts Reported in the Literature

catalyst[a]	BET surface area ($m^2\ g^{-1}$)	mass of the catalyst (mg)	pollutant conc. in ppm and (volume)	degradation: irradiation source	degradation: time (min)	degradation: %	ref
Methylene Blue Degradation							
porous TiO_2(A/R = 85:15)	33.37	10	10 (100 mL)	sunlight	80	100	present work
		10	100 (100 mL)	sunlight	150	43	
		10	500 (100 mL)	sunlight	150	25	
		10	1000 (100 mL)	sunlight	150	12	
TiO_2 nanoflower (A/R = 99:1)	36.9	30	12.79 (150 mL)	UV light	30	100	17
TiO_2 A/B nanoparticles	183.6	60	10 (600 mL)	UV light	180	97	48
TiO_2 rods (A = 100%)	40.5	30	12.79 (150 mL)	UV light	40	80	49
mesoporous TiO_2 (A/B = 80:20)	186	120	32 (200 mL)	UV light	70	100	50
TiO_2 anatase/rutile nanoflowers	106.29	10	15 (20 mL)	350 W xenon lamp	120	72	51
graphene-wrapped anatase−rutile hierarchical TiO_2 nanoflower	33.2	30	500 (40 mL)	500 W Hg lamp	30	100	52
porous TiO_2 (A/R = 55:45)	–	–	1.28 (30 mL)	UV light	100	100	33
$TiO_{2-x}N_x$ heterojunction (A/R = 90:10)	79.6	60	3 (50 mL)	solar simulator	180	90	19
TiO_2 (A = 100) hierarchical mesoporous	159	1.6	10 (8 mL)	UV light	180	90	53
nanocrystalline TiO_2(A = 100)	246	100	100 (100 mL)	sunlight	225	100	38
TiO_2 (A = 100)	29	20	10 (40 mL)	UV light	180	100	18
TiO_2 nanofilms (A = 100%)	–	100	4 (100 mL)	UV light	50	67	54
Methyl Orange Degradation							
porous TiO_2(A/R = 85:15)	33.37	10	10 (100 mL)	sunlight	105	91	present work
core−shell rutile−anatase TiO_2	–	20	10 (150 mL)	UV light	150	100	55
porous TiO_2−Pt−rGO	61.7	20	10 (20 mL)	300 W xenon lamp	120	80	56
TiO_2 nanoflower (A/R = 82:18)	165	300	10 (300 mL)	500 W xenon lamp	60	98	57

catalyst[a]	BET surface area ($m^2\ g^{-1}$)	mass of the catalyst (mg)	conc. of alcohol (mmol)	degradation: irradiation source	degradation: time (min)	degradation: % conversion; selectivity	ref
Benzyl Alcohol Oxidation							
porous TiO_2 (A/R = 85:15)	33.37	10	0.1	sunlight	60	80; 100	present work
CdS/TiO_2	201	8	0.1	500 W xenon lamp	240	45; 97	8
carbonate like doped TiO_2	160	16	0.1	300 W xenon lamp	360	80.6; 99	58
TiO_2−CdS QDs	144	50	0.2	300 W xenon lamp	180	95; 100	9
CdS/TiO_2 composites	42.9	8	0.1	300 W xenon lamp	240	22.3; 100	10
TiO_2 (A = 100%)	210	53	0.1	100 W Hg lamp	240	51; 99	11

[a]A = anatase; R = rutile; and B = brookite.

lowering of the absorption band gap of TiO_2 but also renders the TiO_2 surface hydrophilic due to increased interaction with moisture through hydrogen bonding. The heterojunctions obtained using 350 mg of starch exhibit higher photocatalytic activity in comparison to all other TiO_2 monoliths (Table 2). The highest activity could be as a result of optimum anatase−rutile composition (85:15) and the presence of interstitial carbon as −C−O that aids in better wettability of the catalyst and thus faster interaction and degradation of organics.[6,38,41] TiO_2 prepared using 100 and 200 mg of starch exhibit lower photoactivity (Table 1) due to the low percentage of anatase−rutile heterojunctions (Figure 2). On the other hand, increasing the percentage of anatase−rutile heterojunctions and carbon doping using higher starch content (Table 1) also does not improve the performance of porous TiO_2. Further, the surface areas of TiO_2 prepared using 350 and 2000 mg of starch are comparable. Therefore, the increased solar photocatalytic activity for the heterojunctions can be correlated to the combined effect of the porous network, band gap narrowing due anatase−rutile heterojunctions, and carbon doping. Porous TiO_2 prepared using 350 mg of starch shows better performance in dye degradation under solar light compared to the already known TiO_2-based catalysts (Table 2). In fact, its catalytic activity under sunlight is better than some of the catalysts under UV irradiation. For selective oxidation of benzaldehyde, our catalyst under sunlight performs better than known catalysts under UV light. The enhanced photocatalytic activity under ambient conditions in natural sunlight renders porous TiO_2 monoliths a superior catalyst and a desired material for environmental amelioration.

https://doi.org/10.1021/acsomega.1c00825
ACS Omega 2021, 6, 12124−12132

4. CONCLUSIONS

Solar light active macroporous C-doped TiO_2 heterojunction photocatalysts were prepared through simple, single-step, self-sustained combustion reactions. Porous monoliths of different anatase−rutile ratios (increasing rutile component from 0 to 40%) were obtained by varying the amount of starch. Monoliths with an anatase−rutile ratio of 85:15 exhibit exceptional photocatalytic activity in the degradation of dyes (methylene blue and methyl orange) and selective oxidation of benzyl alcohol to benzaldehyde under natural sunlight. The synthesis route could be used as a general strategy to synthesize economically viable TiO_2 monoliths with multiple features for efficient natural sunlight photocatalytic applications such as H_2 production and CO_2 conversion.

■ ASSOCIATED CONTENT

Supporting Information

The Supporting Information is available free of charge at https://pubs.acs.org/doi/10.1021/acsomega.1c00825.

IR data; graphical representation of the variation of % of rutile with an amount of starch; and table of photocatalytic degradation of the dye and benzyl alcohol oxidation in the presence and absence of porous TiO_2 heterojunctions and sunlight (PDF)

■ AUTHOR INFORMATION

Corresponding Author

C. Nethravathi − *Materials Research Group, Department of Chemistry, St. Joseph's College, Bangalore 560027, India; Department of Chemistry, Mount Carmel College, Bangalore 560052, India;* orcid.org/0000-0002-5000-7417; Email: nethravathic@gmail.com

Authors

R. Ragesh Nath − *Materials Research Group, Department of Chemistry, St. Joseph's College, Bangalore 560027, India*

Michael Rajamathi − *Materials Research Group, Department of Chemistry, St. Joseph's College, Bangalore 560027, India;* orcid.org/0000-0002-4975-1855

Complete contact information is available at: https://pubs.acs.org/10.1021/acsomega.1c00825

Notes

The authors declare no competing financial interest.

■ ACKNOWLEDGMENTS

This work was supported by SERB, India (EMR/2015/001982).

■ REFERENCES

(1) Chen, X.; Mao, S. S. Titanium Dioxide Nanomaterials: Synthesis, Properties, Modifications, and Applications. *Chem. Rev.* **2007**, *107*, 2891−2959.

(2) Wang, Y.; Saitow, K.-I. Mechanochemical Synthesis of Red-Light-Active Green TiO_2 Photocatalysts with Disorder: Defect-Rich, with Polymorphs, and No Metal Loading. *Chem. Mater.* **2020**, *32*, 9190−9200.

(3) Ullattil, S. G.; Ramakrishnan, R. M. Defect-Rich Brown TiO_{2-x} Porous Flower Aggregates: Selective Photocatalytic Reversibility for Organic Dye Degradation. *ACS Appl. Nano Mater.* **2018**, *1*, 4045−4052.

(4) Kaplan, R.; Erjavec, B.; Dražić, G.; Grdadolnik, J.; Pintar, A. Simple synthesis of anatase/rutile/brookite TiO_2 nanocomposite with superior mineralization potential for photocatalytic degradation of water pollutants. *Appl. Catal., B* **2016**, *181*, 465−474.

(5) Wang, W.-K.; Chen, J.-J.; Gao, M.; Huang, Y.-X.; Zhang, X.; Yu, H.-Q. Photocatalytic Degradation of Atrazine by Boron-Doped TiO_2 with a Tunable Rutile/Anatase Ratio. *Appl. Catal., B* **2016**, *195*, 69−76.

(6) Luo, Z.; Poyraz, A. S.; Kuo, C.-H.; Miao, R.; Meng, Y.; Chen, S.-Y.; Jiang, T.; Wenos, C.; Suib, S. L. Crystalline Mixed Phase (Anatase/Rutile) Mesoporous Titanium Dioxides for Visible Light Photocatalytic Activity. *Chem. Mater.* **2015**, *27*, 6−17.

(7) Fukui, M.; Koshidaa, W.; Tanakaa, A.; Hashimotoa, K.; Kominamia, H. Photocatalytic hydrogenation of nitrobenzenes to anilines over noble metal-free TiO_2 utilizing methylamine as a hydrogen donor. *Appl. Catal., B* **2020**, *268*, No. 118446.

(8) Hu, Z.; Quan, H.; Chen, Z.; Shao, Y.; Li, D. New insight into efficient visible-light-driven photocatalytic organic transformation over CdS/TiO_2 photocatalysts. *Photochem. Photobiol. Sci.* **2018**, *17*, 51−59.

(9) Li, X.; Wang, J.; Men, Y.; Bian, Z. TiO_2 mesocrystal with exposed (001) facets and CdS quantum dots as an active visible photocatalyst for selective oxidation reactions. *Appl. Catal., B* **2016**, *187*, 115−121.

(10) Qin, N.; Liu, Y.; Wu, W.; Shen, L.; Chen, X.; Li, Z.; Wu, L. One-Dimensional CdS/TiO_2 Nanofiber Composites as Efficient Visible-Light-Driven Photocatalysts for Selective Organic Transformation: Synthesis, Characterization, and Performance. *Langmuir* **2015**, *31*, 1203−1209.

(11) Zhang, M.; Wang, Q.; Chen, C.; Zang, L.; Ma, W.; Zhao, J. Oxygen Atom Transfer in the Photocatalytic Oxidation of Alcohols by TiO_2: Oxygen Isotope Studies. *Angew. Chem., Int. Ed.* **2009**, *48*, 6081−6084.

(12) Yaemsunthorn, K.; Kobielusz, M.; Macyk, W. TiO_2 with Tunable Anatase-to-Rutile Nanoparticles Ratios: How Does the Photoactivity Depend on the Phase Composition and the Nature of Photocatalytic Reaction? *ACS Appl. Nano Mater.* **2021**, *4*, 633−643.

(13) Zhu, J.; Zhu, S.; Kong, X.; Liang, Y.; Li, Z.; Wu, S.; Luo, S.; Chang, C.; Cui, Z. Rutile-Coated B-Phase TiO_2 Heterojunction Nanobelts for Photocatalytic H_2 Evolution. *ACS Appl. Nano Mater.* **2020**, *3*, 10349−10359.

(14) Gardecka, A. J.; Bishop, C.; Lee, D.; Corby, S.; Parkin, I. P.; Kafizas, A.; Krumdieck, S. High efficiency water splitting photoanodes composed of nano-structured anatase-rutile TiO_2 heterojunctions by pulsed-pressure MOCVD. *Appl. Catal., B* **2018**, *224*, 904−911.

(15) Schneider, J.; Matsuoka, M.; Takeuchi, M.; Zhang, J.; Horiuchi, Y.; Anpo, M.; Bahnemann, D. W. Understanding TiO_2 Photocatalysis: Mechanisms and Materials. *Chem. Rev.* **2014**, *114*, 9919−9986.

(16) Pelaez, M.; Nolan, N. T.; Pillai, S. C.; Seery, M. K.; Falaras, P.; Kontos, A. G.; Dunlope, P. S. M.; Hamiltone, J. W. J.; Byrnee, J. A.; O'Sheaf, K.; Entezarig, M. H.; Dionysioua, D. D. A Review on The Visible Light Active Titanium Dioxide Photocatalysts for Environmental Applications. *Appl. Catal., B* **2012**, *125*, 331−349.

(17) Harris, J.; Silk, R.; Smith, M.; Dong, Y.; Chen, W.-T.; Waterhouse, G. I. N. Hierarchical TiO_2 Nanoflower Photocatalysts with Remarkable Activity for Aqueous Methylene Blue Photo-Oxidation. *ACS Omega* **2020**, *5*, 18919−18934.

(18) Toyoda, M.; Nanbu, Y.; Nakazawa, Y.; Hirano, M.; Inagaki, M. Effect of crystallinity of anatase on photoactivity for methylene blue decomposition in water. *Appl. Catal., B* **2004**, *49*, 227−232.

(19) Etacheri, V.; Seery, M. K.; Hinder, S. J.; Pillai, S. C. Highly Visible Light Active $TiO_{2-x}N_x$ Heterojunction Photocatalysts. *Chem. Mater.* **2010**, *22*, 3843−3853.

(20) Kumaravel, V.; Mathew, S.; Bartlett, J.; Pillai, S. C. Photocatalytic hydrogen production using metal doped TiO_2: A review of recent advances. *Appl. Catal., B* **2019**, *244*, 1021−1064.

(21) Serpone, N. Is the Band Gap of Pristine TiO_2 Narrowed by Anion and Cation-Doping of Titanium Dioxide in Second-Generation Photocatalysts? *J. Phys. Chem. B* **2006**, *110*, 24287−24293.

(22) Asahi, R.; Morikawa, T.; Ohwaki, T.; Aoki, K.; Taga, Y. Visible-Light Induced Photocatalysis in Nitrogen doped Titanium Dioxides. *Science* **2001**, *293*, 269−271.

(23) Pan, X.; Yang, M.-Q.; Fu, X.; Zhang, N.; Xu, Y.-J. Defective TiO_2 with oxygen vacancies: synthesis, properties and photocatalytic applications. *Nanoscale* **2013**, *5*, 3601−3614.
(24) Zhang, X.; Wang, Y.; Liu, B.; Sang, Y.; Liu, H. Heterostructures construction on TiO_2 nanobelts: A powerful tool for building high-performance photocatalysts. *Appl. Catal., B* **2017**, *202*, 620−641.
(25) Bickley, R. I.; Carreno, T. G.; Lee, J. S.; Palmisano, L.; Tilley, R. J. D. A Structural Investigation of Titanium Dioxide Photocatalysts. *J. Solid State Chem.* **1991**, *92*, 178−190.
(26) Scanlon, D. O.; Dunnill, C. W.; Buckeridge, J.; Shevlin, S. A.; Logsdail, A. J.; Woodley, S. M.; Catlow, C. R. A.; Powell, M. J.; Palgrave, R. G.; Parkin, I. P.; Watson, G. W.; Keal, T. W.; Sherwood, P.; Walsh, A.; Sokol, A. A. Band Alignment of Rutile and Anatase TiO_2. *Nat. Mater.* **2013**, *12*, 798−801.
(27) Zhou, X.; Wierzbicka, E.; Liu, N.; Schmuki, P. Black and white anatase, rutile and mixed forms: band-edges and photocatalytic activity. *Chem. Commun.* **2019**, *55*, 533−536.
(28) Hurum, D. C.; Agrios, A. G.; Gray, K. A.; Rajh, T.; Thurnauer, M. C. Explaining the Enhanced Photocatalytic Activity of Degussa P25 Mixed-Phase TiO_2 Using EPR. *J. Phys. Chem. B* **2003**, *107*, 4545−4549.
(29) Pillai, S. C.; Periyat, P.; George, R.; McCormack, D. E.; Seery, M. K.; Hayden, H.; Colreavy, J.; Corr, D.; Hinder, S. J. Synthesis of High-Temperature Stable Anatase TiO_2 Photocatalyst. *J. Phys. Chem. C* **2007**, *111*, 1605−1611.
(30) Sato, S.; Nakamura, R.; Abe, S. Visible-light sensitization of TiO_2 photocatalysts by wet-method N doping. *Appl. Catal., A* **2005**, *284*, 131−137.
(31) Wang, C.; Zhang, X.; Shao, C.; Zhang, Y.; Yang, J.; Sun, P.; Liu, X.; Liu, H.; Liu, Y.; Xie, T.; Wang, D. Rutile TiO_2 nanowires on anatase TiO_2 nanofibers: A branched heterostructured photocatalysts via interface-assisted fabrication approach. *J. Colloid Interface Sci.* **2011**, *363*, 157−164.
(32) Kawahara, T.; Konishi, Y.; Tada, H.; Tohge, N.; Nishii, J.; Ito, S. A Patterned TiO_2(Anatase)/TiO_2(Rutile) Bilayer-Type Photocatalyst: Effect of the Anatase/Rutile Junction on the Photocatalytic Activity. *Angew. Chem., Int. Ed.* **2002**, *41*, 2811−2813.
(33) Su, R.; Bechstein, R.; Sø, L.; Vang, R. T.; Sillassen, M.; Esbjornsson, B.; Palmqvist, A.; Besenbacher, F. How the Anatase-to-Rutile Ratio Influences the Photoreactivity of TiO_2. *J. Phys. Chem. C* **2011**, *115*, 24287−24292.
(34) Liu, Z.; Zhang, X.; Nishimoto, S.; Jin, M.; Tryk, D. A.; Murakami, T.; Fujishima, A. Anatase TiO_2 Nanoparticles on Rutile TiO_2 Nanorods: A Heterogeneous Nanostructure via Layer-by-Layer Assembly. *Langmuir* **2007**, *23*, 10916−10919.
(35) Xing, Z.; Zhang, J.; Cui, J.; Yin, J.; Zhao, T.; Kuang, J.; Xiu, Z.; Wan, N.; Zhou, W. Recent advances in floating TiO_2-based photocatalysts for environmental application. *Appl. Catal., B* **2018**, *225*, 452−467.
(36) Venugopal, B. R.; Samuel, E. P.; Shivakumara, C.; Rajamathi, M. Macroporous metal oxide foams through self-sustained combustion reactions. *J. Porous Mater.* **2009**, *16*, 205−208.
(37) Venugopal, B. R.; Naik, S.; Antony, M.; Ramalingam, G.; Rajamathi, M.; Raghavan, S. Amorphous, Monoclinic, and Tetragonal Porous Zirconia Through a Controlled Self-Sustained Combustion Route. *J. Am. Ceram. Soc.* **2011**, *94*, 1747−1755.
(38) Nagaveni, K.; Hegde, M. S.; Ravishankar, N.; Subbanna, G. N.; Madras, G. Synthesis and Structure of Nanocrystalline TiO_2 with Lower Band Gap Showing High Photocatalytic Activity. *Langmuir* **2004**, *20*, 2900−2907.
(39) Sakthivel, S.; Kisch, H. Daylight Photocatalysis by Carbon-Modified Titanium Dioxide. *Angew. Chem., Int. Ed.* **2003**, *42*, 4908−4911.
(40) Khan, S. U. M.; Al-Shahry, M.; Ingler, W. B., Jr. Efficient Photochemical Water Splitting by a Chemically Modified n-TiO_2. *Science* **2002**, *297*, 2243−2245.
(41) Nagaveni, K.; Sivalingam, G.; Hegde, M. S.; Giridhar, M. Solar photocatalytic degradation of dyes: high activity of combustion synthesized nano TiO_2. *Appl. Catal., B* **2004**, *48*, 83−93.
(42) Hanaor, D. A. H.; Sorrell, C. C. Review of the anatase to rutile phase transformation. *J. Mater. Sci.* **2011**, *46*, 855−874.
(43) Yurdakal, S.; Palmisano, G.; Loddo, V.; Augugliaro, V.; Palmisano, L. Nanostructured Rutile TiO_2 for Selective Photocatalytic Oxidation of Aromatic Alcohols to Aldehydes in Water. *J. Am. Chem. Soc.* **2008**, *130*, 1568−1569.
(44) Brink, G.-J. T.; Arends, I. W. C. E.; Sheldon, R. A. Green, Catalytic Oxidation of Alcohols in Water. *Science* **2000**, *287*, 1636−1639.
(45) Hoffmann, M. R.; Martin, S. T.; Choi, W.; Bahnemann, D. W. Environmental Applications of Semiconductor Photocatalysis. *Chem. Rev.* **1995**, *95*, 69−96.
(46) Mallat, T.; Baiker, A. Oxidation of Alcohols with Molecular Oxygen on Solid Catalysts. *Chem. Rev.* **2004**, *104*, 3037−3058.
(47) Shiraishi, Y.; Saito, N.; Hirai, T. Titanosilicate Molecular Sieve for Size-Screening Photocatalytic Conversion. *J. Am. Chem. Soc.* **2005**, *127*, 8304−8306.
(48) Azeez, F.; Al-Hetlani, E.; Arafa, M.; Abdelmonem, Y.; Nazeer, A. A.; Amin, M. O.; Madkour, M. The Effect of Surface Charge on Photocatalytic Degradation of Methylene Blue Dye Using Chargeable Titania Nanoparticles. *Sci. Rep.* **2018**, *8*, No. 7104.
(49) Chen, W.-T.; Dosado, A. G.; Chan, A.; Waterhouse, D. S.; Waterhouse, G. I. N. Highly Reactive Anatase Nanorod Photocatalysts Synthesized by Calcination of Hydrogen Titanate Nanotubes: Effect of Calcination Conditions on Photocatalytic Performance for Aqueous Dye Degradation and H_2 Production in Alcohol-Water Mixtures. *Appl. Catal., A* **2018**, *565*, 98−118.
(50) Mutuma, B. K.; Shao, G. N.; Kim, W. D.; Kim, H. T. Sol−gel synthesis of mesoporous anatase−brookite and anatase−brookite−rutile TiO_2 nanoparticles and their photocatalytic properties. *J. Colloid Interface Sci.* **2015**, *442*, 1−7.
(51) Xu, H.; Li, G.; Zhu, G.; Zhu, K.; Jin, S. Enhanced Photocatalytic Degradation of Rutile/Anatase TiO_2 Heterojunction Nanoflowers. *Catal. Commun.* **2015**, *62*, 52−56.
(52) Lui, G.; Liao, J.-Y.; Duan, A.; Zhang, Z.; Fowler, M.; Yu, A. Graphene-Wrapped Hierarchical TiO_2 Nanoflower Composites with Enhanced Photocatalytic Performance. *J. Mater. Chem. A* **2013**, *1*, 12255−12262.
(53) Choi, H.; Sofranko, A. C.; Dionysiou, D. D. Nanocrystalline TiO_2 Photocatalytic Membranes with a Hierarchical Mesoporous Multilayer Structure: Synthesis, Characterization, and Multifunction. *Adv. Funct. Mater.* **2006**, *16*, 1067−1074.
(54) Maleki, H.; Bertola, V. TiO_2 Nanofilms on Polymeric Substrates for the Photocatalytic Degradation of Methylene Blue. *ACS Appl. Nano Mater.* **2019**, *2*, 7237−7244.
(55) Wu, M.-C.; Hsiao, K.-C.; Chang, Y.-H.; Kordás, K. Core−Shell Heterostructures of Rutile and Anatase TiO_2 Nanofibers for Photocatalytic Solar Energy Conversion. *ACS Appl. Nano Mater.* **2019**, *2*, 1970−1979.
(56) Huo, J.; Yuan, C.; Wang, Y. Nanocomposites of Three-Dimensionally Ordered Porous TiO_2 Decorated with Pt and Reduced Graphene Oxide for the Visible-Light Photocatalytic Degradation of Waterborne Pollutants. *ACS Appl. Nano Mater.* **2019**, *2*, 2713−2724.
(57) He, Z.; Cai, Q.; Fang, H.; Situ, G.; Qiu, J.; Song, S.; Chen, J. Photocatalytic Activity of TiO_2 Containing Anatase Nanoparticles and Rutile Nanoflower Structure Consisting of Nanorods. *J. Environ. Sci.* **2013**, *25*, 2460−2468.
(58) Yu, L.; Lin, Y.; Li, D. Visible-light-induced aerobic oxidation of alcohols in a green catalytic system of carbonate-like species doped TiO_2. *Appl. Catal., B* **2017**, *216*, 88−94.

https://doi.org/10.1021/acsomega.1c00825
ACS Omega 2021, 6, 12124−12132